Contribution from the Institut für Anorganische Chemie, Universität Bern, CH-3000 Bern 9, Switzerland, Institut Laue Langevin, 38042 Grenoble Cedex, France, Laboratoire d'Optique Physique, ESPCI, 10, Rue Vauquelin, 75231 Paris Cedex 05, France, and Laboratorium für Neutronenstreuung, ETH Zürich, CH-5232 Villigen PSI, Switzerland

Inelastic Neutron Scattering and Optical Absorption Spectroscopy of the $Ti^{2+}(Mn^{2+})_6$ Spin Cluster in Ti^{2+}-Doped $MnBr_2$ and $MnCl_2$

Michael A. Aebersold,[1a] Herma Blank,[1b] Bernard Briat,[1c] Albert Furrer,[1d] and Hans U. Güdel*,[1a]

Received November 27, 1990

$MnCl_2$ and $MnBr_2$ were doped with Ti^{2+} in low concentrations. The $Ti^{2+}(Mn^{2+})_6$ spin clusters thus created were studied by single-crystal absorption spectroscopy in the region of $^3A_{2g} \rightarrow {}^1E_g$ Ti^{2+} and $^6A_{1g} \rightarrow {}^4E_g$, $^4A_{1g}$ Mn^{2+} excitations (D_{3d} notation) as well as by inelastic neutron scattering. Exchange splittings were determined both in the electronic ground state and in the singly excited ^4E_g, $^4A_{1g}$ state. Biquadratic exchange significantly affects the ground-state splitting in Ti^{2+}:$MnBr_2$; $2J_{Ti-Mn} = -7.16$ cm^{-1}, and $j = 0.18$ cm^{-1}. Mn^{2+}–Mn^{2+} exchange can be neglected to a good approximation. In the lowest spin levels of the ground state the ordering has a ferromagnetic appearance, despite the antiferromagnetic nature of the Ti^{2+}–Mn^{2+} exchange. The "large" spins of the six nearest-neighbor Mn^{2+} ions are lined up parallel by the dominant coupling to the "small" Ti^{2+} spin.

1. Introduction

Chemists as well as physicists have shown great interest in exchange-coupled clusters of magnetic ions. These systems serve as simple models for a detailed study of exchange interactions. Chemists in particular have enjoyed studying correlations between various physical properties and chemical and structural variations and to employing molecular concepts for their understanding.[2] In recent years numerous polynuclear complexes containing two different magnetic ions have been synthesized and investigated.[3] With these bimetallic systems a new dimension of chemical variation has been opened up, and novel physical properties have been detected.

We have recently started to prepare bimetallic clusters by codoping two different types of magnetic ions into a diamagnetic host lattice.[4,5] The species thus created usually have very low concentrations. In addition, a whole variety of clusters are created. The conventional techniques used for the study of exchange interactions, such as magnetic susceptibility or heat capacity measurements, are thus not applicable. Spectroscopic techniques, on the other hand, can provide a very high selectivity, so that the various species can be studied individually. Another approach to bimetallic clusters consists in doping a paramagnetic lattice with a magnetic impurity. We have shown for $MnCl_2$ doped with Ti^{2+} that the $Ti^{2+}(Mn^{2+})_6$ clusters thus created can be considered as individual units and their properties can be investigated.[6] This principle only works because the Ti^{2+}–Mn^{2+} interaction is an order of magnitude bigger than the Mn^{2+}–Mn^{2+} interaction.

In the present paper, this earlier work is extended both chemically and methodically. $MnCl_2$ and $MnBr_2$ are doped with various concentrations of Ti^{2+} ions. In Figure 1, we show the three spectroscopic routes to study the $Ti^{2+}(Mn^{2+})_6$ clusters thus obtained. Inelastic neutron scattering (INS) is the first probe. It has been widely applied for the study of exchange interactions in clusters of transition-metal and rare-earth-metal ions.[7-9] INS allows a direct determination of exchange splittings in the ground state, as indicated in Figure 1. Near-infrared (near-IR) optical absorption in the region of $^3A_{2g} \rightarrow {}^1E_g$ (D_{3d} notation) excitations of Ti^{2+} is our second point of attack on the $Ti^{2+}(Mn^{2+})_6$ cluster, and the third one consists of $^6A_{1g} \rightarrow {}^4E_g$, $^4A_{1g}$ excitations on Mn^{2+} in the visible part of the absorption spectrum. As we will show, these techniques are fully complementary, and they allow a rather detailed description of the exchange splittings of the $Ti^{2+}(Mn^{2+})_6$ cluster in both ground and excited states. In addition, they provide some insight into the mechanisms governing the light absorption processes.

Giant spin values up to $S = 16$ are obtained and made accessible to experimental observation in $Ti^{2+}(Mn^{2+})_6$. It is rather difficult to synthesize well-defined molecular polynuclear complexes with levels of such high spin multiplicity. Dodecanuclear manganese complexes with $S = 14$ ground-state levels have recently been reported.[10] On the other hand, a spin cluster very similar to the one studied here has been obtained and investigated by doping Ni^{2+} into MnI_2.[11] In Cr^{3+}-doped $GdAlO_3$ and related compounds the effect of the magnetic order of the host lattice on the ^2E_g and $^4A_{2g}$ states of Cr^{3+} has been investigated.[12,13]

$MnCl_2$ and $MnBr_2$ crystallize in the $CdCl_2$ and CdI_2 structure type, respectively. Space groups are $R\bar{3}m$ and $P\bar{3}m1$, respectively, with unit cell parameters $a = 3.686$ Å and $c = 17.470$ Å for $MnCl_2$ and $a = 3.868$ Å and $c = 6.272$ Å for $MnBr_2$.[14,15] a is the nearest neighbor Mn^{2+}–Mn^{2+} distance within a layer. The Mn^{2+} point group is D_{3d} in both lattices. $MnCl_2$ and $MnBr_2$ undergo transitions to three-dimensional antiferromagnetic order at 1.96 and 2.30 K, respectively.[16] Doping of Ti^{2+} is possible up to a few percent, and the Ti^{2+} ions are assumed to replace Mn^{2+} ions.

2. Experimental Section

Samples of Ti^{2+}:$MnBr_2$ and Ti^{2+}:$MnCl_2$ were obtained by using an in situ reaction to generate the titanium ions.[6] Single crystals were grown by the Bridgman technique at 900 °C with a growth rate of 0.03 mm/min. Polycrystalline samples were synthesized by heating the reaction mixture to 970 °C for 1 h in an electrical furnace. The samples were checked by powder X-ray diffraction, and the titanium concentration was determined colorimetrically.[17]

* To whom correspondence should be addressed.

(1) (a) Universität Bern. (b) Institut Laue-Langevin. (c) ESPCI. (d) ETH Zürich.
(2) Willett, R. D., Gatteschi, D., Kahn, O., Eds. *Magneto-Structural Correlations in Exchange Coupled Systems*; NATO ASI 140; Reidel: Dordrecht, The Netherlands, 1983.
(3) Pei, Y.; Journaux, Y.; Kahn, O. *Inorg. Chem.* **1988**, *27*, 399.
(4) Herren, M.; Jacobsen, S. M.; Güdel, H. U. *Inorg. Chem.* **1989**, *28*, 504.
(5) Herren, M.; Jacobsen, S. M.; Güdel, H. U.; Briat, B. *J. Chem. Phys.* **1989**, *90*, 663.
(6) Jacobsen, S. M.; Güdel, H. U.; Smith, W. E. *Inorg. Chem.* **1987**, *26*, 2001.
(7) Güdel, H. U.; Furrer, A.; Kjems, J. K. *J. Magn. Magn. Mater.* **1986**, *54-57*, 1453 and references therein.
(8) Furrer, A.; Güdel, H. U.; Krausz, E. R.; Blank, H. *Phys. Rev. Lett.* **1990**, *64*, 68 and references therein.
(9) Falk, U.; Furrer, A.; Furer, N.; Güdel, H. U.; Kjems, J. K. *Phys. Rev. B* **1987**, *35*, 4893.
(10) McCusker, J. K.; Schmitt, E. A.; Hendrickson, D. N. *Proceedings of NATO Workshop, Magnetic Molecular Materials*; Gatteschi, D., et al., Eds.; Kluwer Academic Publishers: Dordrecht, The Netherlands, 1991.
(11) Hoekstra, H. J. W. M.; Ronda, C. R.; Haas, C. *Physica* **1983**, *122B*, 295.
(12) Kita, T.; Tanabe, Y. *J. Phys. Soc. Jpn.* **1985**, *54*, 2304 and references therein.
(13) Van der Ziel, J. P.; Van Uitert, L. G. *Phys. Rev. B* **1973**, *8*, 1889.
(14) Wyckoff, R. W. G. *Crystal Structures*, 2nd ed.; Interscience Publishers: New York, 1965; Vol. 1.
(15) *Gmelins Handbuch der Anorganischen Chemie, Mn Teil C 5*; Springer-Verlag: Berlin, 1978; p 268.
(16) Regis, M.; Farge, Y.; Royce, B. S. H. *AIP Conf. Proc.* **1976**, *29*, 654.
(17) *Vogel's Quantitative Chemical Analysis*, 5th ed.; Longman Scientific & Technical: Harlow, England, 1989; p 696.

0020-1669/91/1330-3556$02.50/0

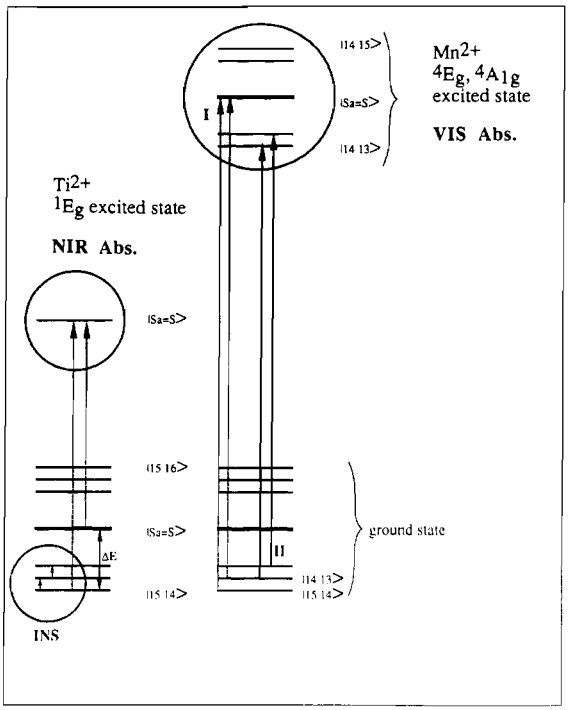

Figure 1. Three different types of spectroscopic transitions measured in this paper: INS, Inelastic neutron scattering transitions within the ground-state multiplet; near-IR absorbance, $^3A_{2g} \rightarrow {}^1E_g$ single excitations on Ti^{2+}; vis absorbance, $^6A_{1g} \rightarrow {}^4E_g, {}^4A_{1g}$ single excitations on Mn^{2+}. Observed transitions, indicated by arrows I and II, are referred to in the text (section 4).

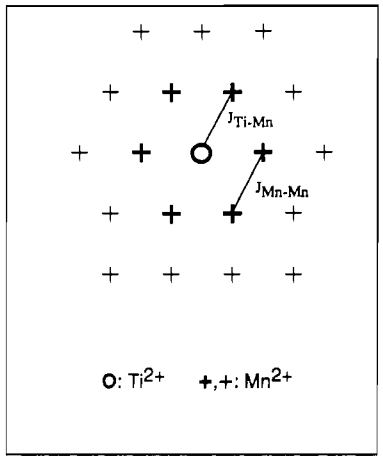

Figure 2. Schematic view of the $Ti^{2+}(Mn^{2+})_6$ cluster in the cation layer of Ti^{2+} doped $MnCl_2$ and $MnBr_2$. J_{Ti-Mn} and J_{Mn-Mn} are the relevant bilinear exchange parameters.

For optical absorption experiments, single crystals of 0.7% Ti^{2+}:$MnBr_2$ and 1% Ti^{2+}:$MnCl_2$ were cleaved along the planes perpendicular to the c axis. The near-IR absorption measurements were done as described elsewhere, with the samples mounted in a helium gas flow tube.[4] Vis absorption spectra were recorded on a home-built double-beam instrument using a liquid-helium-bath cryostat.

The inelastic neutron scattering experiments were done on polycrystalline samples of 7.2% Ti^{2+}:$MnBr_2$ at the reactor Saphir in Würenlingen, Switzerland, and at the Institut Laue-Langevin (ILL) in Grenoble, France. In Würenlingen, Switzerland, a three-axis spectrometer was used in the energy loss configuration with incident neutron energy of 40.3 cm^{-1}. The sample was sealed in an aluminum cylinder of 15 mm diameter and 50 mm length. In Grenoble, France, the time-of-flight instrument IN5 was used with cold neutrons. The wavelength was 5 Å. The sample was sealed in a platelike aluminum container of dimensions 45 × 40 × 4 mm^3.

3. Theory

3.1. Exchange Interactions. Figure 2 shows the $Ti^{2+}(Mn^{2+})_6$ spin cluster to be considered here. It is not a priori clear that this

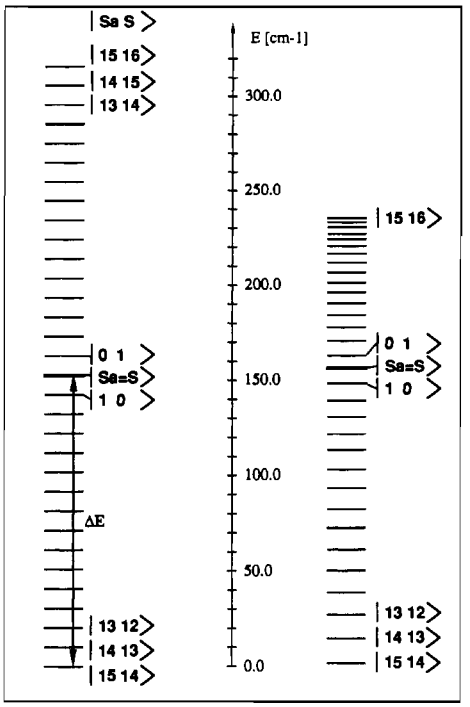

Figure 3. Calculated energy splitting pattern of the $Ti^{2+}(Mn^{2+})_6$ spin cluster. The left side corresponds to bilinear exchange only, eq 1, with $2J = -10.2$ cm^{-1} and $j = 0$; the right side corresponds to bilinear-biquadratic exchange, eq 1, with $2J = -7.16$ cm^{-1} and $j = 0.18$ cm^{-1}.

Scheme I

$$\left.\begin{aligned} S_1 + S_2 &= S_{12} \\ S_3 + S_4 &= S_{34} \end{aligned}\right\} S_{12} + S_{34} = S_{1234} \left.\begin{aligned} &\\ S_5 + S_6 &= S_{56} \end{aligned}\right\} S_{56} + S_{1234} = S_a \left.\begin{aligned} &\\ &\\ S_{Ti} &\end{aligned}\right\} S_a + S_{Ti} = S$$

Scheme II

$$S_{Ti} = 1$$
$$S_i = {}^5/_2 \quad (i = 1, 2, \ldots, 6)$$
$$S_a = 0, 1, \ldots, 15$$
$$S = |S_a - 1|, S_a, |S_a + 1|$$

cluster can be considered as an independent entity in the magnetic lattice of $MnCl_2$ and $MnBr_2$. It will be shown by the experimental results and, in fact, has already been demonstrated for the $MnCl_2$ lattice,[6] that it represents an excellent approximation. Only when we approach the temperature range of magnetic ordering of the host lattice do we observe some significant deviations.

The topology of our $Ti^{2+}(Mn^{2+})_6$ cluster is most simple, with all seven ions lying in the same plane and all the Mn^{2+} ions being crystallographically equivalent. We number the ions $Ti^{2+} = 0$ and the Mn^{2+} ions consecutively from 1 to 6, and we adopt the coupling scheme shown in Scheme I. The corresponding quantum numbers have the values shown in Scheme II. Since in a first approximation the energies of the cluster levels only depend on S_a and S (see below), we can work with a set of basis functions $|S_a S_{Ti} S M\rangle$. The nearest-neighbor Mn^{2+}–Mn^{2+} exchange constant is known to be smaller than 1 cm^{-1} in both $MgCl_2$ and $MgBr_2$.[18] It can therefore be neglected in a good approximation. For Heisenberg exchange the Hamiltonian then takes the very simple form

$$\hat{H}_{ex} = -2J(S_a S_{Ti}) - j(S_a S_{Ti})^2 \qquad (1)$$

where J and j are bilinear and biquadratic exchange parameters, respectively. In eq 1, three-spin interactions are included in the biquadratic term.[9] The energy matrix of this operator is diagonal

(18) Briat, B.; Aebersold, M. A. Unpublished work.

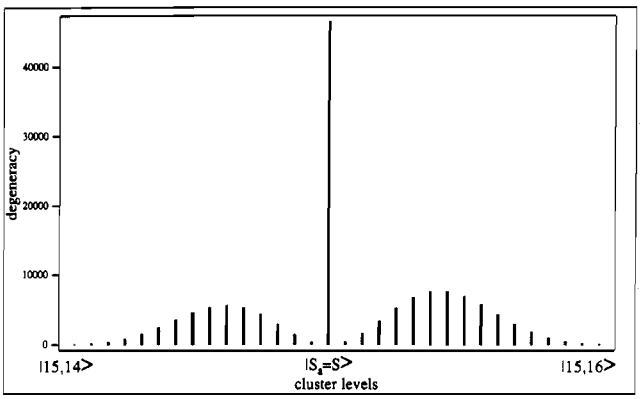

Figure 4. Plot of the degeneracies of the $|S_a,S\rangle$ spin cluster levels.

in a $|S_aS_{Ti}SM\rangle$ basis, and the eigenvalues are easily obtained as

$$E(S_a,S) = -J[S(S+1) - S_a(S_a+1) - 2] - \tfrac{1}{4}j[S(S+1) - S_a(S_a+1) - 2]^2 \quad (2)$$

In Figure 3, the resulting energy level pattern for antiferromagnetic exchange is shown. The left-hand side corresponds to the situation with $j = 0$, i.e. purely bilinear exchange. We note the regular spacing of the levels with an energy difference between adjacent levels of $-2J$. This is in contrast to the Landé splitting pattern obtained for dimers with a Hamiltonian of the type shown in eq 1. The effect of the biquadratic term is shown on the right-hand side of Figure 3. The spacing between adjacent levels decreases with increasing energy for $j > 0$.

Since the energies do not depend on the quantum numbers S_{12}, S_{34}, S_{56}, S_{1234}, and M, there is a great deal of degeneracy in this splitting pattern, which is diagrammatically shown in Figure 4. The level $|S_a = S\rangle$ has about the same total degeneracy as all the other levels together. It acquires a high Boltzmann population at relatively low temperatures and thus becomes observable in an absorption spectrum.

3.2. Inelastic Neutron Scattering (INS). INS transitions are possible between the exchange-split levels of the ground state. Their intensity is governed by the differential scattering cross section. Such cross sections have been evaluated for various dimers, trimers, and tetramers.[7] For a transition

$$|\{[(S_1S_2)S_{12}(S_3S_4)S_{34}]S_{1234}(S_5S_6)S_{56}\}S_aS_{Ti}S\rangle \rightarrow |\{[(S_1S_2)S'_{12}(S_3S_4)S'_{34}]S'_{1234}(S_5S_6)S'_{56}\}S'_aS_{Ti}S'\rangle$$

in our $Ti^{2+}(Mn^{2+})_6$ spin cluster it is given by

$$\frac{d^2\sigma}{d\Omega\, d\omega} = CF^2(\mathbf{Q}) \exp\left(-\frac{E(S_a,S)}{k_bT}\right)\sum_{\alpha\beta}\left(\delta_{\alpha\beta} - \frac{Q_\alpha Q_\beta}{Q^2}\right) \times \sum_{ij}\exp\{i\mathbf{Q}(\mathbf{R}_i - \mathbf{R}_j)\} \times \sum_{MM'}\langle S_aSM|\hat{S}_i^\alpha|S_a'S'M'\rangle\langle S_a'S'M'|\hat{S}_j^\beta|S_aSM\rangle \times \delta\{\hbar\omega + E(S_a,S) - E(S_a',S')\} \quad (3)$$

with

$$C = \frac{N}{Z}\left(\frac{\gamma e^2}{m_ec^2}\right)^2\frac{k_1}{k_0}\exp\{-2W\}$$

where $\mathbf{Q}$ is the scattering vector, $F(\mathbf{Q})$ the magnetic form factor, $\mathbf{R}_i$ ($i = 0$–6) the position vector of the ion i in the cluster, N the number of clusters in the sample and Z the partition function. k_0 and k_1 are the wavenumbers of incoming and scattered neutrons, respectively, $\exp\{-2W\}$ is the Debye–Waller factor, and α and β stand for the coordinates x, y, and z. The remaining symbols have their usual meaning.[19] The evaluation of this cross section is not trivial mainly due to the matrix elements and the geometry factors

(19) Marshall, W.; Lovesey, S. W. *Theory of Thermal Neutron Scattering*; Clarendon Press: Oxford, England 1971; Chapter 5.

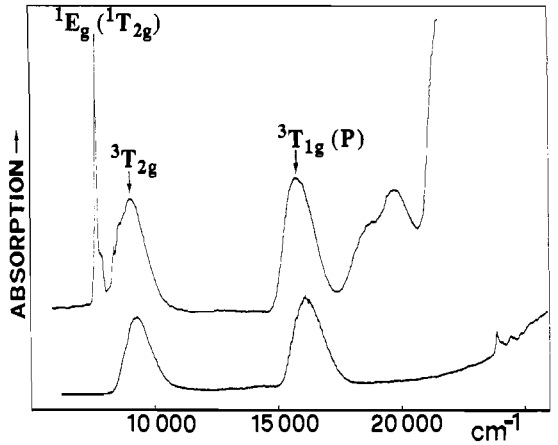

Figure 5. Near-IR and part of the vis absorption spectra at 10 K of single crystals of $MgCl_2$ doped with 5% of Ti^{2+} (lower trace) and $MnCl_2$ doped with 1% of Ti^{2+} (upper trace). Adapted from ref 21.

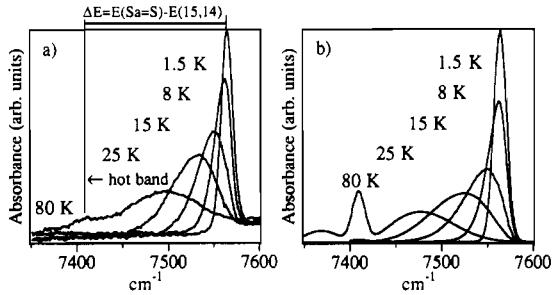

Figure 6. (a) Experimental (0.7% Ti^{2+} in $MnBr_2$) and (b) calculated temperature dependence of Ti^{2+} $^3A_{2g} \rightarrow {}^1E_g$ excitations in the spin cluster $Ti^{2+}(Mn^{2+})_6$, corresponding to the near-IR transitions in Figure 1. $2J = -7.16$ cm^{-1} and $j = 0.18$ cm^{-1} were used for the calculation, assuming Gaussian shapes with half-widths of the 1.5 K spectrum. The energy difference between the cold band (1.5 K) at 7564 cm^{-1} and the hot band at 7411 cm^{-1} corresponds to ΔE in Figure 1.

$\sum_{ij}exp\{i\mathbf{Q}(\mathbf{R}_i - \mathbf{R}_j)\}$. The $|S_aS_{Ti}SM\rangle$ basis functions are multiply coupled, see Scheme I, whereas the operators $\hat{S}_i^\alpha$ are single-ion operators. Tensor operator techniques were therefore used for the evaluation of matrix elements. Since all the experiments were carried out on powdered samples, the cross section formula had to be integrated in Q space. The derivation of the final formula is lengthy and will not be given here. It is available on request.[20]

For a transition

$$|\{(S_{12}S_{34})S_{1234}S_{56}\}S_aS_{Ti}S\rangle \rightarrow |\{(S'_{12}S'_{34})S'_{1234}S'_{56}\}S'_aS_{Ti}S'\rangle$$

the cross section is given by

$$\frac{d^2\sigma}{d\Omega\, d\omega} = CF^2(\mathbf{Q})\exp\left(-\frac{E(S_a,S)}{k_bT}\right)\delta\{\hbar\omega + E(S_a,S) - E(S_a',S')\}\frac{1}{3}\sum_{i=1}^{10}A_i \quad (4)$$

where the complicated terms A_i are given in Table IV. This formula will be used for the calculation of relative intensities in section 4. More important are perhaps the selection rules, which can be derived from formula 4. There are numerous selection rules concerning ΔS_{12}, ΔS_{34}, ΔS_{56}, and ΔS_{1234} that are unimportant for a qualitative discussion. The following general selection rules are important:

$$\Delta S = 0, \pm 1 \qquad \Delta M = 0, \pm 1 \quad (5)$$

$$\Delta S_a = 0, \pm 1 \qquad \Delta M_a = 0, \pm 1$$

In terms of the splitting pattern shown in Figure 3, we thus have three types of INS transitions: (1) $\Delta S = \pm 1$ and $\Delta S_a = \pm 1$

(20) Aebersold, M. A. Diplomarbeit, University of Bern, 1989.

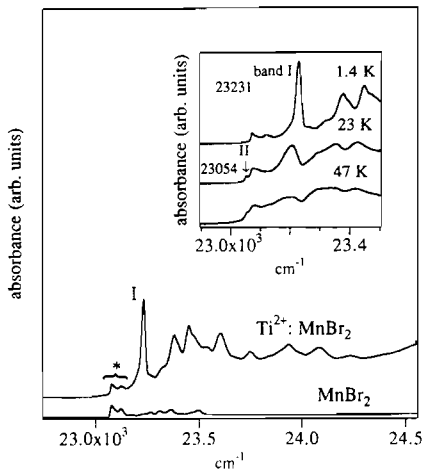

Figure 7. Single-crystal absorption spectra at 1.4 K of pure $MnBr_2$ (lower trace) and 0.7% Ti^{2+}:$MnBr_2$ (upper trace) in the region of $^6A_{1g} \rightarrow {}^4E_g, {}^4A_{1g}$ excitations. Origins of $MnBr_2$ and $Ti^{2+}(Mn^{2+})_6$ spin cluster transitions are marked with an asterisk and I, respectively. The insert shows the temperature dependence of the origin region. Bands I and II refer to the corresponding transitions in Figure 1.

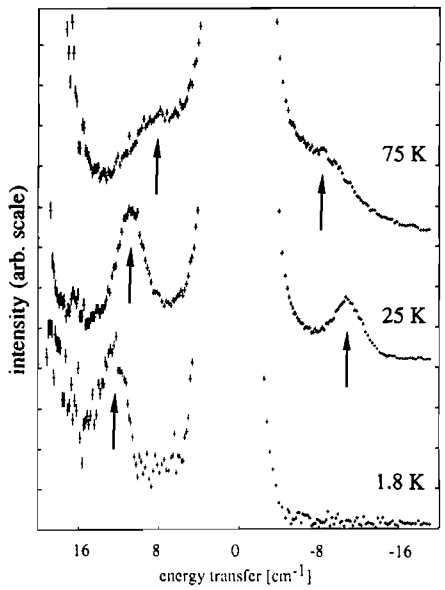

Figure 8. Time-of-flight inelastic neutron scattering spectra of a polycrystalline sample of 7.2% Ti^{2+}:$MnBr_2$ as a function of temperature. The measurements were performed on the instrument IN5 at the Institut Laue-Langevin, Grenoble, France, by using $\lambda = 5$ Å and summing over all scattering angles. The peak positions for energy loss (left side) and energy gain (right side) are indicated with arrows.

transitions between adjacent levels; (2) $\Delta S = 0$ and $\Delta S_a = \pm 1$ or $\Delta S = \pm 1$ and $\Delta S_a = 0$ transitions to the highly degenerate levels $|S_a = S\rangle$; (3) $\Delta S = \pm 1$ and $\Delta S_a = \mp 1$ transitions $|S_a,S\rangle \leftrightarrow |S'_a = S,S' = S_a\rangle$ between the wings. The latter two types are outside our experimental range, so we concentrate on the transitions between adjacent levels, which provide a direct measure of the strength of the exchange coupling; see arrows in Figure 1.

4. Results

Figure 5 shows a section of the near-IR and vis single-crystal low-temperature absorption spectra of Ti^{2+} in $MgCl_2$ and $MnCl_2$.[21] The $^3A_{2g} \rightarrow {}^1E_g$ (D_{3d} notation) of Ti^{2+} is not observable in $MgCl_2$ due to its extremely low oscillator strength ($f \simeq 4 \times 10^{-9}$).[22] In contrast, the same transition leads to a very prominent sharp absorption band in $MnCl_2$ and $MnBr_2$. The intensity increases

(21) Jacobsen, S. M.; Güdel, H. U. *J. Lumin.* **1987**, *38*, 184.
(22) Jacobsen, S. M.; Güdel, H. U.; Daul, C. A. *J. Am. Chem. Soc.* **1988**, *110*, 7610.

Table I. Experimental and Calculated INS Peak Positions and Half-Widths (fwhm) as a Function of Temperature[a]

	peak pos, cm^{-1}			fwhm, cm^{-1}	
	expt				
T, K	loss	gain	calcn	expt	calcn
1.8	12.7 ± 0.4		12.7	3.4 ± 0.4	3.4
4.0	12.2 ± 0.4		12.7	3.4 ± 0.4	3.4
8.0	11.9 ± 0.4	−11.9 ± 0.5	12.5	3.6 ± 0.4	3.5
25.0	10.9 ± 0.4	−10.8 ± 0.5	10.8	3.8 ± 0.4	4.0
40.0	10.1 ± 0.5	−10.1 ± 0.5	10.2	4.3 ± 0.6	4.1
55.0	9.9 ± 0.5	−9.9 ± 0.6	9.8	4.5 ± 0.6	4.2
75.0	9.0 ± 0.6	−9.0 ± 0.6	9.6	4.5 ± 0.6	4.7

[a] Equation 4, $2J = -7.16$ cm^{-1}, and $j = 0.18$ cm^{-1} were used for the calculation, assuming Gaussian shapes for each transition with the half-widths of the 1.8 K experimental transition.

Table II. Experimental and Calculated INS Intensities (in Arbitrary Units) for Energy Gain as a Function of the Modulus of the Scattering Vector Q[a]

Q, Å^{-1}	expt	calcn
0.13	0.58 ± 0.15	0.63
0.41	1.00 ± 0.25	0.86
0.76	0.97 ± 0.24	1.05
1.13	0.88 ± 0.22	0.95
1.49	0.79 ± 0.20	0.83
1.87	0.62 ± 0.16	0.65
2.18	0.62 ± 0.16	0.56

[a] $T = 25.0$ K. The calculation was scaled to the experimental values by a least-squares fit.

Table III. Experimental and Calculated INS Intensities (in Arbitrary Units) for Energy Loss and Energy Gain as a Function of Temperature[a]

	intensity energy loss		intensity energy gain	
T, K	expt	calcn	expt	calcn
1.8	0.81 ± 0.22	0.23		0.0
4.0	0.64 ± 0.16	0.23		0.03
8.0	0.66 ± 0.17	0.30	0.23 ± 0.06	0.06
25.0	1.00 ± 0.25	1.00	1.00 ± 0.25	1.00
40.0	1.08 ± 0.27	1.26	1.47 ± 0.37	1.63
55.0	1.01 ± 0.25	1.31	1.87 ± 0.47	1.89
75.0	1.28 ± 0.32	1.29	2.41 ± 0.60	2.02

[a] Equation 4, $2J = -7.16$ cm^{-1}, and $j = 0.18$ cm^{-1} were used for the calculation. Calculation and experiment were scaled to one for $T = 25$ K.

by at least 3 orders of magnitude on going from the nonmagnetic host $MgCl_2$ to the paramagnetic $MnCl_2$ and $MnBr_2$ lattices. This intensity increase is the result of the Ti^{2+}–Mn^{2+} exchange interactions, and the corresponding mechanism was first proposed by Tanabe.[23,24]

The temperature dependence of the $^3A_{2g} \rightarrow {}^1E_g$ absorption band in 0.7% Ti^{2+}:$MnBr_2$ is shown in Figure 6a. It exhibits an unusual broadening and shift to lower energy with increasing temperature. This is a result of the exchange splitting in the ground state as will be analyzed in section 5. Above 60 K a hot band situated at 7411 cm^{-1} with a relatively narrow bandwidth is observed. In Ti^{2+}:$MnCl_2$ the overall behavior is very similar, but the sharp hot band is more pronounced.[6]

Figure 7 shows the region of $^6A_{1g} \rightarrow {}^4E_g, {}^4A_{1g}$ excitations in the 1.4 K single-crystal absorption spectra of 0.7% Ti^{2+}:$MnBr_2$ and pure $MnBr_2$. The spectrum of the doped crystal is dominated by absorption bands that are absent in pure $MnBr_2$ and that we therefore associate with the $Ti^{2+}(Mn^{2+})_6$ spin cluster. Considering the low doping level of 0.7% Ti^{2+}, there is an increase by about 3 orders of magnitude of the $^6A_{1g} \rightarrow {}^4E_g, {}^4A_{1g}$ intensity compared to pure $MnBr_2$. This is reminiscent of the intensity increase observed for the $^3A_{2g} \rightarrow {}^1E_g$ excitation of Ti^{2+} in $MnCl_2$ and $MnBr_2$. It is clearly due to a Tanabe mechanism.[23,24] The insert of Figure 7 shows the low-energy side of the $^6A_{1g} \rightarrow {}^4E_g, {}^4A_{1g}$ spectrum as a function of temperature. The hot band arising below the prominent cold origin I is marked II, and it will be assigned

Table IV. Derivation[a] of Eq 4 Leading to 10 Different Terms A_i[20]

$$A_1 = \delta(S_a,S'_a)\,(12)(2S+1)(2S'+1)\begin{Bmatrix} S & S' & 1 \\ 1 & 1 & S_a \end{Bmatrix}^2$$

$$A_2 = \delta(S_a,S'_a)\,\delta(S_{12},S'_{12})\,\delta(S_{34},S'_{34})\,\delta(S_{56},S'_{56})\,(-1)^{S+S'+S_a+S_{1234}+S'_{1234}+S_{34}+S_{56}}\,8\sqrt{315}(2S+1)(2S'+1)(2S_a+1)\times$$
$$\sqrt{(2S_{1234}+1)(2S'_{1234}+1)}(2S_{12}+1)\begin{Bmatrix} S & S' & 1 \\ 1 & 1 & S_a \end{Bmatrix}\begin{Bmatrix} S & S' & 1 \\ S_a & S_a & 1 \end{Bmatrix}\begin{Bmatrix} S_a & S_a & 1 \\ S'_{1234} & S_{1234} & S_{56} \end{Bmatrix}\begin{Bmatrix} S_{1234} & S'_{1234} & 1 \\ S_{12} & S_{12} & S_{34} \end{Bmatrix}\begin{Bmatrix} S_{12} & S_{12} & 1 \\ \frac{1}{2} & \frac{1}{2} & \frac{1}{2} \end{Bmatrix}\left[\frac{\sin(QR)}{QR}\right]$$

$$A_3 = \delta(S_a,S'_a)\,\delta(S_{12},S'_{12})\,\delta(S_{34},S'_{34})\,\delta(S_{56},S'_{56})\times$$
$$(-1)^{S+S'+S_a+S_{12}+S_{34}}\,8\sqrt{315}(2S+1)(2S'+1)(2S_a+1)\sqrt{(2S_{1234}+1)(2S'_{1234}+1)}(2S_{34}+1)\times$$
$$\begin{Bmatrix} S & S' & 1 \\ 1 & 1 & S_a \end{Bmatrix}\begin{Bmatrix} S & S' & 1 \\ S_a & S_a & 1 \end{Bmatrix}\begin{Bmatrix} S_a & S_a & 1 \\ S'_{1234} & S_{1234} & S_{56} \end{Bmatrix}\begin{Bmatrix} S_{1234} & S'_{1234} & 1 \\ S_{34} & S_{34} & S_{12} \end{Bmatrix}\begin{Bmatrix} S_{34} & S_{34} & 1 \\ \frac{1}{2} & \frac{1}{2} & \frac{1}{2} \end{Bmatrix}\left[\frac{\sin(QR)}{QR}\right]$$

$$A_4 = \delta(S_a,S'_a)\,\delta(S_{1234},S'_{1234})\,\delta(S_{56},S'_{56})\,(-1)^{S+S'+S_a+S_{1234}+1}\,8\sqrt{315}(2S+1)(2S'+1)(2S_a+1)(2S_{56}+1)\times$$
$$\begin{Bmatrix} S & S' & 1 \\ 1 & 1 & S_a \end{Bmatrix}\begin{Bmatrix} S & S' & 1 \\ S_a & S_a & 1 \end{Bmatrix}\begin{Bmatrix} S_a & S_a & 1 \\ S_{56} & S_{56} & S_{1234} \end{Bmatrix}\begin{Bmatrix} S_{56} & S_{56} & 1 \\ \frac{1}{2} & \frac{1}{2} & \frac{1}{2} \end{Bmatrix}\left[\frac{\sin(QR)}{QR}\right]$$

$$A_5 = \delta(S_{34},S'_{34})\,\delta(S_{56},S'_{56})\,(210)(2S+1)(2S'+1)(2S_a+1)(2S'_a+1)(2S_{1234}+1)(2S'_{1234}+1)(2S_{12}+1)(2S'_{12}+1)\times$$
$$\begin{Bmatrix} S & S' & 1 \\ S'_a & S_a & 1 \end{Bmatrix}^2\begin{Bmatrix} S_a & S'_a & 1 \\ S'_{1234} & S_{1234} & S_{56} \end{Bmatrix}^2\begin{Bmatrix} S_{1234} & S'_{1234} & 1 \\ S'_{12} & S_{12} & S_{34} \end{Bmatrix}^2\begin{Bmatrix} S_{12} & S'_{12} & 1 \\ \frac{1}{2} & \frac{1}{2} & \frac{1}{2} \end{Bmatrix}^2\left[1+(-1)^{S_{12}-S'_{12}}\frac{\sin(QR)}{QR}\right]$$

$$A_6 = \delta(S_{12},S'_{12})\,\delta(S_{56},S'_{56})\,(210)(2S+1)(2S'+1)(2S_a+1)(2S'_a+1)(2S_{1234}+1)(2S'_{1234}+1)(2S_{34}+1)(2S'_{34}+1)\times$$
$$\begin{Bmatrix} S & S' & 1 \\ S'_a & S_a & 1 \end{Bmatrix}^2\begin{Bmatrix} S_a & S'_a & 1 \\ S'_{1234} & S_{1234} & S_{56} \end{Bmatrix}^2\begin{Bmatrix} S_{1234} & S'_{1234} & 1 \\ S'_{34} & S_{34} & S_{12} \end{Bmatrix}^2\begin{Bmatrix} S_{34} & S'_{34} & 1 \\ \frac{1}{2} & \frac{1}{2} & \frac{1}{2} \end{Bmatrix}^2\left[1+(-1)^{S_{34}-S'_{34}}\frac{\sin(QR)}{QR}\right]$$

$$A_7 = \delta(S_{1234},S'_{1234})\,(210)(2S+1)(2S'+1)(2S_a+1)(2S'_a+1)(2S_{56}+1)(2S'_{56}+1)\times$$
$$\begin{Bmatrix} S & S' & 1 \\ S'_a & S_a & 1 \end{Bmatrix}^2\begin{Bmatrix} S_a & S'_a & 1 \\ S'_{56} & S_{56} & S_{1234} \end{Bmatrix}^2\begin{Bmatrix} S_{56} & S'_{56} & 1 \\ \frac{1}{2} & \frac{1}{2} & \frac{1}{2} \end{Bmatrix}^2\left[1+(-1)^{S_{56}-S'_{56}}\frac{\sin(QR)}{QR}\right]$$

$$A_8 = \delta(S_{12},S'_{12})\,\delta(S_{34},S'_{34})\,\delta(S_{56},S'_{56})\,(-1)^{S_{1234}+S'_{1234}+S_{12}+S_{34}}\times$$
$$(105)(2S+1)(2S'+1)(2S_a+1)(2S'_a+1)(2S_{1234}+1)(2S'_{1234}+1)(2S_{12}+1)(2S_{34}+1)\times$$
$$\begin{Bmatrix} S & S' & 1 \\ S'_a & S_a & 1 \end{Bmatrix}^2\begin{Bmatrix} S_a & S'_a & 1 \\ S'_{1234} & S_{1234} & S_{56} \end{Bmatrix}^2\begin{Bmatrix} S_{1234} & S'_{1234} & 1 \\ S_{12} & S_{12} & S_{34} \end{Bmatrix}\begin{Bmatrix} S_{1234} & S'_{1234} & 1 \\ S_{34} & S_{34} & S_{12} \end{Bmatrix}\times$$
$$\begin{Bmatrix} S_{12} & S_{12} & 1 \\ \frac{1}{2} & \frac{1}{2} & \frac{1}{2} \end{Bmatrix}\begin{Bmatrix} S_{34} & S_{34} & 1 \\ \frac{1}{2} & \frac{1}{2} & \frac{1}{2} \end{Bmatrix}\left[\frac{2\sin(QR)}{QR}+\frac{4\sin(\sqrt{3}QR)}{\sqrt{3}QR}+\frac{\sin(2QR)}{QR}\right]$$

$$A_9 = \delta(S_{1234},S'_{1234})\,\delta(S_{34},S'_{34})\,\delta(S_{56},S'_{56})\,(-1)^{S_a+S'_a+S_{1234}+S_{12}+S'_{12}+S_{34}+S_{56}+1}\times$$
$$(105)(2S+1)(2S'+1)(2S_a+1)(2S'_a+1)(2S_{1234}+1)(2S_{56}+1)\sqrt{(2S_{12}+1)(2S'_{12}+1)}\times$$
$$\begin{Bmatrix} S & S' & 1 \\ S'_a & S_a & 1 \end{Bmatrix}^2\begin{Bmatrix} S_a & S'_a & 1 \\ S_{1234} & S_{1234} & S_{56} \end{Bmatrix}\begin{Bmatrix} S_{1234} & S_{1234} & 1 \\ S'_{12} & S_{12} & S_{34} \end{Bmatrix}\begin{Bmatrix} S_{12} & S'_{12} & 1 \\ \frac{1}{2} & \frac{1}{2} & \frac{1}{2} \end{Bmatrix}\times$$
$$\begin{Bmatrix} S_a & S'_a & 1 \\ S_{56} & S_{56} & S_{1234} \end{Bmatrix}\begin{Bmatrix} S_{56} & S_{56} & 1 \\ \frac{1}{2} & \frac{1}{2} & \frac{1}{2} \end{Bmatrix}\left[\frac{2\sin(\sqrt{3}QR)}{\sqrt{3}QR}+\frac{2\sin(QR)}{QR}+(-1)^{S_{12}-S'_{12}}\left(\frac{\sin(2QR)}{QR}+\frac{2\sin(\sqrt{3}QR)}{\sqrt{3}QR}\right)\right]$$

$$A_{10} = \delta(S_{1234},S'_{1234})\,\delta(S_{12},S'_{12})\,\delta(S_{56},S'_{56})\,(-1)^{S_a+S'_a+S_{1234}+S_{12}+S_{56}+1}\times$$
$$(105)(2S+1)(2S'+1)(2S_a+1)(2S'_a+1)(2S_{1234}+1)(2S_{56}+1)\sqrt{(2S_{34}+1)(2S'_{34}+1)}\times$$
$$\begin{Bmatrix} S & S' & 1 \\ S'_a & S_a & 1 \end{Bmatrix}^2\begin{Bmatrix} S_a & S'_a & 1 \\ S_{1234} & S_{1234} & S_{56} \end{Bmatrix}\begin{Bmatrix} S_{1234} & S_{1234} & 1 \\ S'_{34} & S_{34} & S_{12} \end{Bmatrix}\begin{Bmatrix} S_{34} & S'_{34} & 1 \\ \frac{1}{2} & \frac{1}{2} & \frac{1}{2} \end{Bmatrix}\times$$
$$\begin{Bmatrix} S_a & S'_a & 1 \\ S_{56} & S_{56} & S_{1234} \end{Bmatrix}\begin{Bmatrix} S_{56} & S_{56} & 1 \\ \frac{1}{2} & \frac{1}{2} & \frac{1}{2} \end{Bmatrix}\left[\frac{2\sin(\sqrt{3}QR)}{\sqrt{3}QR}+\frac{\sin(2QR)}{QR}+(-1)^{S_{34}-S'_{34}}\left(\frac{2\sin(QR)}{QR}+\frac{2\sin(\sqrt{3}QR)}{\sqrt{3}QR}\right)\right]$$

[a] In these expressions, the curly brackets are $6-j$ symbols and the expressions in square brackets are the so-called interference terms.[27]

and discussed in section 5. Band I shows a broadening and red-shift with increasing temperature quite similar to the near-IR band around 7550 cm^{-1} shown in Figure 6.

Figure 8 illustrates the results of the INS experiments. The inelastic peaks are marked by arrows. They are clearly resolved up to about 50 K, and above this temperature, we observe considerable broadening. The left-hand side of the spectra is the energy-loss-side, corresponding to the excitation of the sample by the neutron beam, and the right-hand side is the energy-gain side. In a Raman spectrum, the two regions would be called Stokes and anti-Stokes, respectively. In Tables I and III, the positions and intensities of the inelastic peaks are listed for all the seven experimental temperatures between 1.8 and 75 K. There is a pronounced shift of the peak position to lower energy with in-

(23) Ferguson, J.; Guggenheim, H. J.; Tanabe, Y. *J. Phys. Soc. Jpn.* **1966**, *21*, 692.
(24) Gondaira, K. I.; Tanabe, Y. *J. Phys. Soc. Jpn.* **1966**, *21*, 1527.

creasing temperature, which is also evident from Figure 8. Table II lists the Q dependence of the peak intensity in energy gain at 25 K.

5. Discussion

In ref 6, it was shown that the concept of an isolated Ti^{2+}-$(Mn^{2+})_6$ spin cluster could successfully account for the temperature dependence of the $^3A_{2g} \leftrightarrow {}^1E_g$ absorption and luminescence spectrum of Ti^{2+} in $MnCl_2$ around 7700 cm^{-1}. For a bilinear Heisenberg exchange Hamiltonian, a value $2J = -12.4$ cm^{-1} was obtained for the Ti^{2+}–Mn^{2+} exchange parameter.

As a result of a much broader data base, we are now in a position to check the model very rigorously. $MnCl_2$ and $MnBr_2$ are structurally and magnetically closely related, and also the optical spectroscopic properties of Ti^{2+}-doped crystals are very similar. For inelastic neutron scattering experiments, $MnBr_2$ is better suited, because chlorine atoms belong to the elements showing significant incoherent scattering.[25] As we will show below, the INS technique provides the most direct clues concerning the applicability of the model. That is why we concentrated on the $MnBr_2$ host in this study, although our conclusions should also be valid for Ti^{2+}-doped $MnCl_2$. With reference to Figure 1, we can equate $\Delta E = E(S_a{=}S) - E(15,14)$ with the energy difference between the two transitions in the near-IR absorption spectrum marked by arrows. This is the $\Delta E = 153$ cm^{-1} between the cold and hot bands in Figure 6. According to the bilinear Heisenberg model, Figure 3(left), ΔE equals $-30J$, so that we get $2J = -10.2$ cm^{-1} for $MnBr_2$. This is the same technique by which $2J = -12.4$ cm^{-1} was obtained for the Ti^{2+}–Mn^{2+} interaction in Ti^{2+}:$MnCl_2$.

INS transitions measure the energy difference between adjacent spin levels. We should thus observe an INS peak at 10.2 cm^{-1} independent of temperature if the bilinear model is valid. From Figure 8 and Table I, we see that this is only approximately true. The inelastic peak does occur around 10.2 cm^{-1}, but the peak position shifts from 12.7 cm^{-1} at 1.8 K to about 9 cm^{-1} at 75 K. This decrease of the INS excitation energy with increasing temperature is a clear indication that the splitting pattern is not equidistant as shown on the left-hand side of Figure 3, but rather corresponds to the right-hand side of Figure 3. This pattern was obtained by including the biquadratic term in eq 1. $2J$ and j were obtained by equating the theoretical energy difference ΔE with the experimental value of 153 cm^{-1} obtained from the vis absorption and the energy difference $E(14,13) - E(15,14)$ with the 1.8 K INS peak position of 12.7 cm^{-1}. The result is

$$2J = -7.16 \text{ cm}^{-1} \qquad (6)$$

$$j = 0.18 \text{ cm}^{-1}$$

With these parameters, the positions and widths of the INS transitions were calculated for the seven experimental temperatures. As Table I shows, the agreement with the measured positions is good.

Using the cross section formula (4) the dependence of the INS intensity was calculated as a function of Q, the modulus of the scattering vector. As shown in Table II there is reasonable agreement at 25 K between the experimental and the calculated Q dependence. The temperature dependence of the INS intensity was also calculated by using eq 4 and the parameter values in eq 6 (Table III). The agreement with the experimental values is acceptable for temperatures above 8 K, but at the lowest temperatures, the measured intensity is significantly higher than the calculated one. We ascribe this to a breakdown of our $Ti^{2+}(Mn^{2+})_6$ spin cluster approximation. Two-dimensional spin correlations are important up to much higher temperatures than the three-dimensional ordering temperature of 2.3 K. Our notion of an independent $Ti^{2+}(Mn^{2+})_6$ spin cluster loses its validity as we approach the magnetic ordering temperature. Our results show that the INS intensities are much more affected by this onset of magnetic order in the host lattice than the energy differences.

(25) Bacon, G. E. *Neutron Scattering in Chemistry*; Butterworth & Co.: London, 1977; p 179.

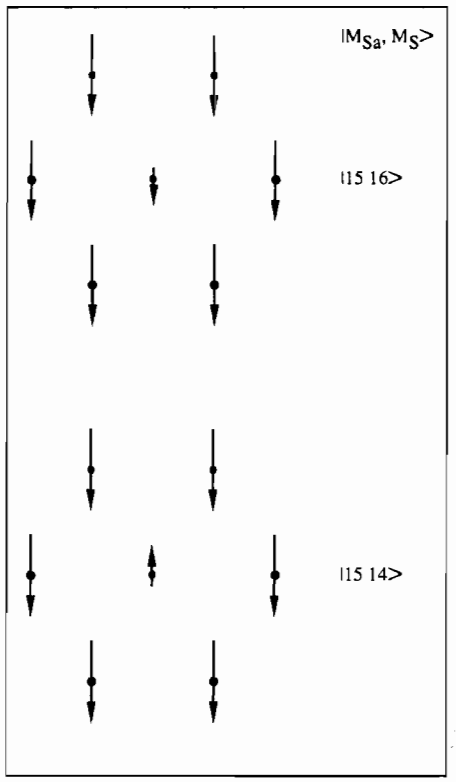

Figure 9. Schematic representation of the most stable and least stable spin configurations $|15,14\rangle$ and $|15,16\rangle$, respectively. The Ti^{2+}–Mn^{2+} interaction is antiferromagnetic.

Scheme III

$$S_{Ti} = 1$$
$$S_i = {}^5/_2 \ (i = 1, \ldots, j-1, j+1, \ldots, 6)$$
$$S_j = {}^3/_2$$
$$S_a^{exc} = 0, 1, \ldots, 14$$
$$S^{exc} = |S_a^{exc} - 1|, S_a^{exc}, |S_a^{exc} + 1|$$

We now turn to a discussion of the absorption spectra. At 1.5 K, only the $|15,14\rangle$ level is populated. The 1.5 K absorption spectrum in Figure 6a thus corresponds to a transition from the lowest spin level $|15,14\rangle$ to $|S_a = S\rangle$ levels of the ^1E_g excited state. We assume that, according to the Tanabe intensity mechanism, $\Delta S = 0$ and $\Delta S_a = 0, \pm 1$ selection rules are operative.[23,24] Since Ti^{2+} is in a singlet state, there is no exchange splitting in the $|S_a = S\rangle$ ^1E_g spin-cluster state as long as we can neglect Mn^{2+}–Mn^{2+} coupling. The change in band shape and position observed in Figure 6 upon increasing the temperature is therefore the result of an increasing population of the higher energy spin levels of the ground-state multiplet. From the parameter values in eq 6 and the bandwidth of the 1.5 K spectrum, the spectra in Figure 6b were calculated. The agreement with the experimental behavior is remarkable and confirms the essential correctness of the spin-cluster model. There is one notable discrepancy between the experimental and calculated spectrum at 80 K. The sharp hot band with its associated low-energy tail is considerably broadened and possibly somewhat weaker in the experimental spectrum. This broadening, which is also observed in Ti^{2+}:$MnCl_2$, but to a lesser degree, is another indication that our spin-cluster model is only approximately true. The $(S_a = S)$ levels in the ground and excited state are strictly degenerate only when J_{Mn-Mn} is exactly zero. Values of $2J_{Mn-Mn} \cong -0.36$ and -0.24 cm^{-1} were determined for Mn^{2+}–Mn^{2+} dimers in the host lattices $MgCl_2$ and $MgBr_2$, respectively.[18] As a consequence of a nonvanishing J_{Mn-Mn} value the $(S_a = S)$ levels are energetically split, resulting in the observed broadening of the $(S_a = S) \rightarrow (S_a^{exc} = S^{exc})$ absorption band.

When we consider a $^6A_{1g} \rightarrow {}^4E_g, {}^4A_{1g}$ Mn^{2+} excitation of our spin cluster, the situation is slightly more complicated because the excited state is also split by Ti^{2+}–Mn^{2+} exchange interactions.

A $^6A_{1g} \rightarrow {}^4E_g, {}^4A_{1g}$ transition on Mn^{2+} corresponds to a simple spin-flip within the ground state configuration $(t_{2g})^3(e_g)^2$ (O_h notation). We can thus ignore, as we did for the ground state, the orbital part and simply couple the spins.[23] Using the same coupling scheme as for the ground state (see Scheme I), we obtain values shown in Scheme III for the quantum numbers. The range of values for the quantum numbers S_a and S is reduced by one compared to the ground state, and we can schematically draw the splitting pattern shown on the top of Figure 1. In this simplified procedure, we have neglected the effect of excitation transfer. Excitations on the six Mn^{2+} ions are energetically equivalent. They do not represent proper eigenstates of the spin cluster. The proper eigenstates correspond to symmetry-adapted linear combinations of the six locally excited configurations transforming like $A_{1g} + B_{1u} + E_{2g} + E_{1u}$ in the D_{6h} spin-cluster symmetry. Their energies will depend on the magnitude of the excitation transfer integrals between neighboring Mn^{2+} ions.[23] For our present discussion, however, the simplified picture is sufficient. With the selection rules $\Delta S = 0$ and $\Delta S_a = 0, \pm 1$ the two types of transitions I and II shown in Figure 1 are observable, as seen in Figure 7. Band I broadens and shifts to lower energy with increasing temperature as a consequence of populating higher ground-state spin levels. The band at 23 054 cm^{-1} has a temperature dependence corresponding to the Boltzmann population of the $|14,13\rangle$ ground-state level and can thus be assigned to transition II. Its position, 173 cm^{-1} below band I at 1.4 K, can be used to determine the effective J value in the excited state. Within the bilinear approximation, we get

$$2J(^4E_g, {}^4A_{1g}) = -11.6 \text{ cm}^{-1} \quad (7)$$

In Ti^{2+}:$MnCl_2$ the same behavior is observed. The energy difference between bands I and II is 212 cm^{-1}. For the J value in the excited state, we thus get

$$2J(^4E_g, {}^4A_{1g}) = -14.3 \text{ cm}^{-1} \quad (8)$$

Both values are slightly higher than the values of $2J = -10.2$ and -12.4 cm^{-1} obtained by the same approximation for the ground states in Ti^{2+}:$MnBr_2$ and Ti^{2+}:$MnCl_2$, respectively. This is very reasonable when we consider the fact that both the ground and excited state derive from the same strong-field electron configuration on Mn^{2+}. For Mn^{2+}-Mn^{2+} pairs in $CsMgCl_3$ and $CsMgBr_3$, it was found that exchange interactions in the ^4E_g, $^4A_{1g}$ states were about 33% stronger than those in the ground state.[26]

Finally we want to comment on the general appearance of the spin level structure in such a bimetallic cluster; see Figures 3 and 4. It consists of three distinct parts: the degenerate or nearly degenerate ($S_a = S$) levels, a low-energy wing, which may be expanded by biquadratic exchange, consisting of $(S + 1, S)$ spin levels and a high-energy wing, which may be compressed by biquadratic exchange, consisting of $(S - 1, S)$ levels. Within the low-energy wing the spin level ordering has a ferromagnetic appearance despite the antiferromagnetic nature of the Ti^{2+}-Mn^{2+} exchange. This at first sight paradoxical result arises from the topology and the dominance of Ti^{2+}-Mn^{2+} exchange in our $Ti^{2+}(Mn^{2+})_6$ spin cluster. It can be visualized as shown in Figure 9. $|M_{S_a}, M_S\rangle = |15,14\rangle$ and $|15,16\rangle$ represent the most stable and the least stable configurations of the seven spins for antiferromagnetic Ti^{2+}-Mn^{2+} interaction. The "small" Ti^{2+} spin is thus able to line up all the "large" Mn^{2+} spins in a ferromagnetic-like fashion. This is, of course, the same principle that governs ferrimagnetism in magnetically ordered systems. In this sense the spin cluster studied here can be considered as a ferrimagnetic cluster. With six Mn^{2+} ions surrounding Ti^{2+}, we obtain unusually high spin quantum numbers.

Acknowledgment. We are grateful to Stuart Jacobsen for his help, for many useful discussions, and for providing a crystal. This work was financially supported by the Swiss National Science Foundation and the CNRS of France.

Registry No. $MnCl_2$, 7773-01-5; $MnBr_2$, 13446-03-2; Ti^{2+}, 15969-58-1; Mn^{2+}, 16397-91-4; neutron, 12586-31-1.

(26) McCarthy, P. J.; Güdel, H. U. *Inorg. Chem.* **1984**, *23*, 880.
(27) Furrer, A.; Güdel, H. U. *Phys. Rev. Lett.* **1977**, *39*, 657.

Notes

Contribution from the Department of Chemistry, Monash University, Clayton, Victoria 3168, Australia, and Department of Physical and Inorganic Chemistry, University of Adelaide, Adelaide, South Australia 5001, Australia

Manganese(III) Complexes of a Binucleating Schiff-Base Ligand Based on the 1,3-Diaminopropan-2-ol Backbone

Karen Bertoncello,[1a] Gary D. Fallon,[1a] Keith S. Murray,*[,1a] and Edward R. T. Tiekink[1b]

Received September 12, 1990

As part of our interest in the structural, magnetic,[2,3] and bioinorganic chemical properties[4,5] of manganese complexes, we report here an interesting group of manganese(III) complexes formed with the potentially binucleating ligand 2-OH-SALPN. We had earlier studied binuclear species of this ligand and related ones, with a range of transition-metal ions,[6-9] and our studies of

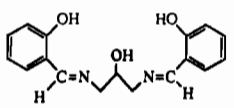

2-OH-SALPN

manganese complexes coincided with a similar study by Pecoraro and Hatfield et al. the results of which have recently been published.[10] Since some of the products were the same, only a brief discussion will be given here of these materials, with emphasis being placed on new aspects not covered by Pecoraro et al.[10] Compounds not obtained by this group will also be highlighted here. In particular, we describe a Na^+-linked polymeric species $[Mn(2\text{-OH-SALPN})(OAc)(NaClO_4)(MeCN)]_x$ (**6**), containing chains of 6-coordinate Mn(III) centers bridged by 7-coordinate Na^+ ions via bridging acetate linkages. This is different in detail

(1) (a) Monash University. (b) University of Adelaide.
(2) Butler, K. D.; Murray, K. S.; West, B. O. *Aust. J. Chem.* **1971**, *24*, 2249.
(3) Kennedy, B. J.; Murray, K. S. *Inorg. Chem.* **1985**, *24*, 1552.
(4) Toftlund, H.; Markiewicz, A.; Murray, K. S. *Acta Chem. Scand.* **1990**, *44*, 443.
(5) Bertoncello, K.; Fallon, G. D.; Murray, K. S. *Inorg. Chim. Acta* **1990**, *174*, 57.
(6) Mazurek, W.; Berry, K. J.; Murray, K. S.; O'Connor, M. J.; Snow, M. R.; Wedd, A. G. *Inorg. Chem.* **1982**, *21*, 3071.
(7) Mazurek, W.; Kennedy, B. J.; Murray, K. S.; O'Connor, M. J.; Rodgers, J. R.; Snow, M. R.; Wedd, A. G.; Zwack, P. R. *Inorg. Chem.* **1985**, *24*, 3258.
(8) Dutton, J. C.; Tiekink, E. R. T.; Murray, K. S. *Inorg. Chim. Acta* **1989**, *166*, 5.
(9) Fallon, G. D.; Markiewicz, A.; Murray, K. S.; Quach, T. *J. Chem. Soc., Chem. Commun.* **1991**, 198.
(10) (a) Bonadies, J. A.; Kirk, M. L.; Lah, M. S.; Kessissoglou, D. P.; Hatfield, W. E.; Pecoraro, V. L. *Inorg. Chem.* **1989**, *28*, 2037. (b) Bonadies, J. A.; Maroney, M. J.; Pecoraro, V. L. *Inorg. Chem.* **1989**, *28*, 2044.

0020-1669/91/1330-3562$02.50/0